Journal of Power Sources 208 (2012) 328–339

Contents lists available at SciVerse ScienceDirect

Journal of Power Sources

journal homepage: www.elsevier.com/locate/jpowsour

Generalized flooded agglomerate model for the cathode catalyst layer of a polymer electrolyte membrane fuel cell

Sai Kamarajugadda, Sandip Mazumder*

Department of Mechanical and Aerospace Engineering, The Ohio State University, Columbus, OH 43210, USA

ARTICLE INFO

Article history:
Received 14 December 2011
Received in revised form 16 February 2012
Accepted 18 February 2012
Available online 25 February 2012

Keywords:
Polymer electrolyte membrane
Flooded agglomerate
Cathode catalyst layer
Modeling
Oxygen reduction reaction
ORR

ABSTRACT

The flooded agglomerate model has found prolific usage in modeling the oxygen reduction reaction within the cathode catalyst layer of a polymer electrolyte membrane fuel cell (PEMFC). The assumption made in this model is that the ionomer-coated carbon–platinum agglomerate is spherical in shape and that the spheres are non-overlapping. This assumption is convenient because the governing equations lend themselves to closed-form analytical solution when a spherical shape is assumed. In reality, micrographs of the catalyst layer show that the agglomerates are best represented by sets of overlapping spheres of unequal radii. In this article, the flooded agglomerate is generalized by considering overlapping spheres of unequal radii. As a first cut, only two overlapping spheres are considered. The governing reaction-diffusion equations are solved numerically using the unstructured finite-volume method. The volumetric current density is extracted for various parametric variations, and tabulated. This sub-grid-scale generalized flooded agglomerate model is first validated and finally coupled to a computational fluid dynamics (CFD) code for predicting the performance of the PEMFC. Results show that when the agglomerates are small (<200 nm equivalent radius), the effect of agglomerate shape on the overall PEMFC performance is insignificant. For large agglomerates, on the other hand, the effect of agglomerate shape was found to be critical, especially for high current densities for which the mass transport resistance within the agglomerate is strongly dependent on the shape of the agglomerate, and was found to correlate well with the surface-to-volume ratio of the agglomerate.

1. Introduction

One of the major impediments to commercial success of hydrogen–oxygen fuel cells is the cost associated with the excessive use of platinum within the catalyst layers. In a polymer electrolyte membrane fuel cell (PEMFC), since the catalyst (platinum) is dispersed within a complex porous matrix comprised of carbon, the ionomer (Nafion) and platinum, the performance of the fuel cell has a convoluted relationship with an increase in the amount of platinum within the catalyst layer. Rather than the amount of platinum, the performance depends on how the platinum is dispersed within the porous matrix so that it is effectively utilized in catalyzing the electrochemical reactions. Thus, there is strong motivation for optimization of the catalyst layers of a PEMFC. Since the proper functioning of a PEMFC cathode requires existence of triple phase boundaries [1,2] between the ionomer (for proton transfer), platinum (for catalysis) and carbon (for electron transfer), the determination of optimum composition and structure of the catalyst layer is a monumental task. Such studies are often undertaken using experiments [3,4], but are very time-consuming and expensive. Computational modeling provides an alternative pathway to address this critical issue.

Model-based optimization of the cathode catalyst layer of a PEMFC has been a topic of intense research over the past two decades. Models used for this purpose may be broadly categorized as: (1) models that utilize the pseudo-homogeneous film concept [5–9], or the flooded agglomerate concept [10–28], and (2) direct numerical simulation (DNS) of the catalyst layer [29–33]. While the latter approach is more first-principles and general, it is usually performed at a much smaller scale and is cumbersome for coupling to a device-scale model. First, it requires reconstruction of the catalyst layer microstructure from micrographs. Secondly, direct numerical solution of the transport-reaction equations within the complex catalyst layer structure are difficult to perform and are very expensive. Simulation times for a single case may often run into days. This makes this approach impractical for engineering calculations. Nevertheless, direct numerical simulations are very useful for fundamental understanding of the coupling between transport and reactions at the pore scale of the cathode catalyst layer.

* Corresponding author at: Department of Mechanical and Aerospace Engineering, The Ohio State University, Suite E410, Scott Laboratory, 201 West 19th Avenue, Columbus, OH 43210, USA. Tel.: +1 614 247 8099; fax: +1 614 292 3163.
E-mail address: mazumder.2@osu.edu (S. Mazumder).

0378-7753/$ – see front matter © 2012 Elsevier B.V. All rights reserved.
doi:10.1016/j.jpowsour.2012.02.063

Nomenclature

A_f	area of face f of control volume (m^2)
A_v	total catalyst surface area per unit volume of anode or cathode (m^{-1})
c	dissolved oxygen concentration in Nafion ($kmol\,m^{-3}$)
c^*	dissolved oxygen concentration in Nafion in equilibrium with inlet gas ($kmol\,m^{-3}$)
c_0^{ref}	standard reference oxygen concentration ($kmol\,m^{-3}$)
$c_{O_2,g}$	oxygen gas concentration in cathode gas pores ($kmol\,m^{-3}$)
$c^*_{O_2,g}$	oxygen gas concentration at cathode inlet ($kmol\,m^{-3}$)
$\bar{d}$	average pore size of cathode (m)
$\mathcal{D}_{kn}$	binary diffusion coefficient of species k into n ($m^2\,s^{-1}$)
D_λ	diffusion coefficient of water ($m^2\,s^{-1}$)
D'_λ	concentration dependence of D_λ, dimensionless
D_T	temperature dependence of D_λ, ($m^2\,s^{-1}$)
$D_{O_2,N}$	diffusion coefficient of oxygen in Nafion ($m^2\,s^{-1}$)
$D^{eff}_{O_2,N}$	effective diffusion coefficient of oxygen in Nafion in agglomerate ($m^2\,s^{-1}$)
F	Faraday's constant ($96.487 \times 10^6\,C\,kmol^{-1}$)
$\mathbf{i}$	net current density vector ($A\,m^{-2}$)
$\mathbf{i}_F$	ionic phase current density vector ($A\,m^{-2}$)
i_0^{ref}	standard exchange current density on cathode ($A\,m^{-3}$)
$\mathbf{i}_S$	electronic phase current density vector ($A\,m^{-2}$)
i_s^{cat}	surface current density on catalyst surface of cathode ($A\,m^{-2}$)
$\mathbf{J}_k$	diffusion mass flux of the kth species ($kg\,m^{-2}\,s^{-1}$)
j_T^{an}	net transfer current at anode ($A\,m^{-3}$)
j_T^{cat}	net transfer current density at cathode ($A\,m^{-3}$)
j_0	reference current density ($A\,m^{-2}$)
L	cathode catalyst layer thickness (m)
m_{Pt}	platinum mass loading ($kg\,m^{-2}$)
M_m	molar mass of the membrane ($kg\,kmol^{-1}$)
M_k	molecular weight of kth species ($kg\,kmol^{-1}$)
n	number of electrons transferred during the electrochemical reaction
$\widehat{n}$	number of agglomerates per unit volume of cathode (m^{-3})
$\hat{\mathbf{n}}_f$	unit surface normal at control volume face
N	total number of gas-phase species
p	pressure (Pa)
Pt|C	platinum–carbon mass ratio in catalyst layer ink, dimensionless
r_{agg}	radius (actual or equivalent) of agglomerate (m)
r_1, r_2	radii of the two overlapping spheres (m)
R	universal gas constant ($8314\,J\,kmol^{-1}\,K^{-1}$)
$\dot{S}_k$	production rate of kth species ($kg\,m^{-3}\,s^{-1}$)
T	absolute temperature (K)
U	bulk fluid velocity ($m\,s^{-1}$)
V_{agg}	total volume of agglomerate (m^3)
V_{nuc}	volume of nucleus of agglomerate (m^3)
V_{ctg}	volume of coating (m^3)
V_O	volume of cell or control volume O (m^3)
Y_k	mass fraction of kth species

Greek

α_a, α_c	Tafel constants for anode, dimensionless
α_T	Tafel constant for cathode catalyst model, dimensionless
β_k	concentration exponents for the kth species
δ	polymer coating thickness around agglomerate nucleus (m)
ε	wet porosity, dimensionless
ε_{agg}	volume fraction of polymer in agglomerate nucleus, dimensionless
ε_{cat}	porosity of cathode catalyst layer, dimensionless
ε_S	volume fraction of platinum + carbon in cathode, dimensionless
ε_N	volume fraction of polymer in cathode, dimensionless
η	electrode overpotential (V)
η_d	electro-osmotic drag coefficient, dimensionless
κ	permeability (m^2)
λ	water content, dimensionless
$[\Lambda_k]$	molar concentration of species k ($kmol\,m^{-3}$)
μ	dynamic viscosity ($kg\,m^{-1}\,s^{-1}$)
ρ	mass density of mixture ($kg\,m^{-3}$)
ρ_m^{dry}	density of dry membrane ($kg\,m^{-3}$)
σ	electrical conductivity ($\Omega^{-1}\,m^{-1}$)
σ_F	electrical conductivity of the ionic phase ($\Omega^{-1}\,m^{-1}$)
σ_S	electrical conductivity of the electronic phase ($\Omega^{-1}\,m^{-1}$)
σ_{30}	concentration dependence of electrical conductivity ($\Omega^{-1}\,m^{-1}$)
ϕ_F	ionic phase potential (V)
ϕ_S	electronic phase potential (V)
ϕ_{OC}	open circuit voltage (V)
τ_{cat}	tortuosity of cathode, dimensionless
ξ	overlap parameter, dimensionless

The more popular approach is based on hypothesized models of coupled mass transport and reactions within the catalyst layer structure. Historically, two different model types have been used for this purpose. The first model type, generally referred to in the literature as the pseudo-homogeneous film model [5–9], assumes that the catalyst layer is a porous matrix comprised of Nafion, platinum, and carbon in random (homogeneous) configuration. This model allows for pathways of gases, electrons, and protons within the catalyst layer, and captures some of the essential transport phenomena prevalent in the catalyst layer. However, this model does not acknowledge the necessity for the existence of the triple-phase boundary for a functioning catalyst layer. In contrast, the flooded agglomerate concept, proposed in the late 1980s [10,11], contends that the platinum is supported on carbon particles, which forms agglomerates when mixed with an ionomer. The agglomerate may even be coated fully or partially by an additional ionomer layer. The oxygen finds its way to the platinum by first dissolving in the ionomer, and is consumed as it transports to the core of the carbon–platinum aggregate. This model guarantees the existence of triple-phase boundaries as long as sufficient amounts of the ionomer are present. Calculations performed using this model appear to match experimental data better than the pseudo-homogeneous film model [8,19]. Most notable among early studies that have used the flooded agglomerate model is the work of Jaouen et al. [15,16,34], Sun et al. [18], and Secanell et al. [19], although this model has found prolific usage more recently. Jaouen et al. have successfully used this model to predict the performance of the cathode as a function of operating conditions and cathode layer thicknesses. Their calculations predicted experimentally observed double Tafel slopes [16], attributed to local (within agglomerate) mass

transport limitations. However, the model was not exercised to study effect of other compositional variables such as Nafion loading and platinum loading. Such studies were performed by Sun et al. [18], who predicted an optimum Nafion loading—consistent with experimentally observed behavior [3,4]. Studies performed by both Sun et al. [18] and Secanell et al. [19] suggests that the performance of the cathode improves monotonically as the agglomerate radius is decreased. However, it is believed [30,31] that excessive reduction in the agglomerate radius can lead to severe reduction in the size of the macropores and high tortuosity. This, in turn, can result in deterioration of the performance, especially at high current densities, due to global mass transport limitations. A more general form of the flooded agglomerate model that accounts all of the afore-stated issues was proposed by Kamarajugadda and Mazumder [35], and has been used thereafter by other researchers [27,28].

One of the main assumptions in the flooded agglomerate model is that the agglomerates are spherical in shape, and that the spheres are non-overlapping or spatially isolated. While there is sufficient evidence from micrographs [36] to suggest the predominance of spherical shape of the agglomerates (presumably because surface tension tends to make them spherical), there is little evidence to suggest that these spheres are spatially isolated. In a recent study, Jain et al. [37] have shown significant differences at the agglomerate-scale in the effectiveness of oxygen consumption between plate-like, spherical, and cylindrical agglomerates. They attribute this to the differences in the resistance to oxygen diffusion between agglomerates and within the agglomerates for different shapes. Careful examination of micrographs seem to suggest that the agglomerates may be most closely likened to groups of overlapping spheres of unequal radii, much like clusters of soap bubbles that have partially coalesced. It is worth noting that the assumption of spatially isolated spherical agglomerates stems from the fact that under this assumption, the governing reaction-diffusion equation at the agglomerate scale can be conveniently solved using analytical techniques, which makes the model easy to implement in a large-scale model for prediction of the overall performance of a PEMFC. The assumption is not necessarily driven by observations of reality, and therefore, there is a pressing need to assess its validity.

In this study, the flooded agglomerate model is generalized to account for agglomerate shape effects. Specifically, based on the rationale presented earlier and as part of this preliminary investigation, agglomerates represented by two overlapping spheres of unequal radii is considered, although the model presented here can be used for agglomerates of arbitrary shape and size. In addition, two different shapes of ionomer coating are also considered. The governing reaction-diffusion equation at the agglomerate scale is solved numerically using the unstructured finite-volume procedure for variations of relevant parameters that govern the catalyst layer's composition. The numerical solutions are post-processed to extract volumetric current densities, and are then tabulated for subsequent use. The agglomerate-scale model is first validated against analytical solutions, and subsequently incorporated in a full-scale computational fluid dynamics (CFD) code for the prediction of the performance of the full PEMFC, thereby resulting in a generalized multi-scale model of the PEMFC.

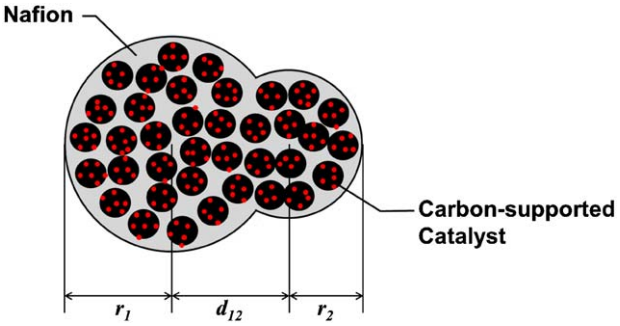

Fig. 2. Agglomerate nucleus represented by two overlapping spheres of unequal radii with carbon-supported (black) catalyst particles (red dots) distributed in the polymer electrolyte (gray). (For interpretation of the references to color in this figure legend, the reader is referred to the web version of the article.)

2. Model description

Computational modeling of a PEMFC entails sub-division of the entire fuel cell (or computational domain) into smaller control volumes (or cells), and subsequently solving equations of conservation of mass, momentum, energy, and charge for each control volume. The sub-divided network of control volumes, referred to as a mesh or grid, is necessary to spatially resolve all quantities of interest. Since the catalyst layer of a PEMFC has features that are less than a micron in size, while the fuel cell itself is of the order of a few centimeters in size, it is impossible to resolve these features within the catalyst layer by the same mesh that is used to model the full PEMFC. Thus, a separate model is necessary at the catalyst layer scale, and is referred to as the sub-grid scale model. This sub-grid scale model has to be ultimately coupled with the larger scale model in order to study the impact of small-scale physics on the device-scale performance. The relationship between the various scales is depicted schematically in Fig. 1.

2.1. Sub-grid scale agglomerate model

The cathode catalyst layer consists of three components: the solid carbon–platinum clusters, the polymer electrolyte (or ionomer), and gas pores. For the sub-grid scale agglomerate model to be valid, the agglomerate size must be sufficiently small compared to the cathode layer thickness such that the electric potential within an agglomerate may be assumed to be constant. Transport of reactants from the cathode channel to the cathode active layer is dominated by diffusion within the pores of the cathode diffusion layer and the cathode catalyst layer (see Fig. 1). Oxygen reaches platinum within the agglomerate by dissolution into the

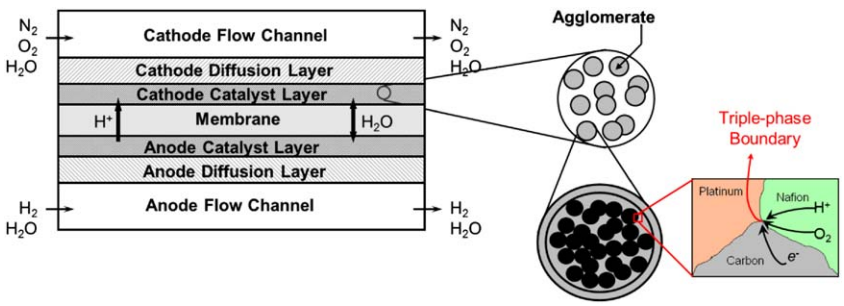

Fig. 1. Schematic representation of the cross-section of a PEM fuel cell showing the various length scales involved and their relationship.

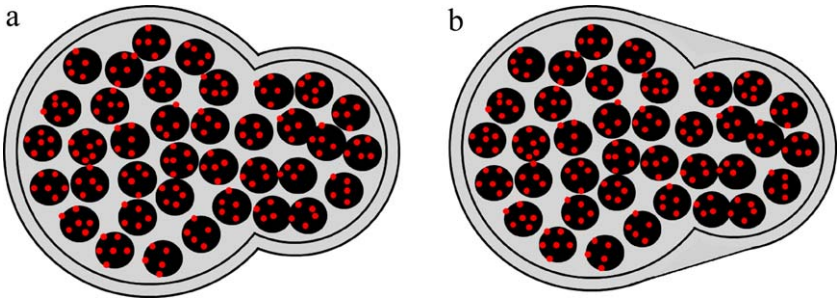

Fig. 3. Coating configurations for intersecting sphere agglomerate nucleus: (a) thin coating and (b) capsule coating.

polymer coating followed by diffusion through the polymer within the agglomerate. The objective of the sub-grid scale model is to provide the volumetric current density generated by a unit volume of the catalyst layer by taking into account the effect platinum loading, Nafion loading, platinum-to-carbon ratio, and the microstructure of the catalyst layer. As discussed in Section 1, the so-called flooded agglomerate model has been used routinely for this purpose.

In the generalized flooded agglomerate model proposed here, the cathode is assumed to be comprised of a large number of agglomerates formed by two overlapping spheres of equal or unequal radii (Fig. 2). In such a scenario, the shape of the agglomerate can be characterized by the radii of the two intersecting spheres, r_1 and r_2, and the so-called overlap parameter, ξ. The overlap parameter is another measure of the distance between the center of the two overlapping spheres, d_{12}, which may be written as

$$d_{12} = r_1 + \xi r_2 \tag{1}$$

where $-1 \le \xi \le 1$. $\xi = -1$ represents a single sphere of radius r_1 ($>r_2$), while $\xi = 1$ represents the two spheres just touching each other. Each agglomerate is comprised of clusters of carbon-supported platinum particles held together by a proton-conducting polymer. The agglomerate may be coated with a thin film of polymer. In this study, two different coating shapes are considered (Fig. 3): (a) a coating of uniform thickness following the contour of the agglomerate nucleus surface, and (b) a thin uniform coating around part of the curved nucleus surface, with a conical frustum of thicker layer connecting the two thin sections. Henceforth, the first coating configuration is referred to as "thin coating," while the second configuration is referred to as "capsule coating." For both these coating configurations, "coating thickness (δ)" refers to the value of thickness of the uniform coating around the curved surface of the agglomerate nucleus. Therefore, for the same prescribed value of coating thickness, the capsule coating case for a given agglomerate nucleus has a higher volume of polymer in the coating than the thin coating case. While the proposed model is not in complete agreement with observed microstructures of the catalyst layer, it represents the next logical extension of an isolated-sphere flooded agglomerate model that has been in use thus far.

2.1.1. Agglomerate model governing equation

Within the agglomerate, oxygen is assumed to diffuse through the polymer electrolyte to the catalyst surface. While it diffuses through the nucleus of the agglomerate, it reacts on the platinum clusters impregnated on the carbon surfaces, and is consumed (Fig. 2). For an agglomerate of arbitrary shape, the reaction-diffusion balance equation for dissolved oxygen concentration in Nafion, c, is given by [10,11]:

$$\nabla \cdot (D^{\text{eff}}_{O_2,N} \nabla c) + \gamma \frac{A_v i^{\text{cat}}_s (1 - \varepsilon_{\text{agg}})}{nF} = 0 \tag{2}$$

where $\gamma = 1$ in the nucleus and $\gamma = 0$ in the coating, A_v represents the total catalyst surface area per unit volume of cathode catalyst layer available for the oxygen reduction reaction (ORR) [18,19], i^{cat}_s is the surface current density the catalyst surface, and ε_{agg} is the volume fraction of polymer present within the agglomerate nucleus. n is the number of electrons transferred during the ORR (=2 for a H_2/O_2 PEMFC), and F is the Faraday constant. The ORR kinetics is assumed to follow a Tafel law, and to be first-order in oxygen concentration. Hence, the surface current density on the catalyst surface is given by [15]:

$$i^{\text{cat}}_s = -i^{\text{ref}}_0 \left(\frac{c^*}{c^{\text{ref}}_{O_2}} \right)^{1-\alpha_T/n} \exp\left(-\frac{\alpha_T F}{RT} \eta \right) \frac{c}{c^*} \tag{3}$$

where $c^{\text{ref}}_{O_2}$ is the standard reference oxygen concentration, i^{ref}_0 is the standard exchange current density for a smooth catalyst surface, and η is the local overpotential defined as the difference between the electronic and protonic phase potentials, *i.e.*, $\eta = \phi_S - \phi_F$. c and c^* are the dissolved oxygen concentration in the polymer at the catalyst surface and the dissolved oxygen concentration in the polymer in equilibrium with the inlet gas, respectively. Substitution of Eq. (3) in Eq. (2) results in a linear partial differential equation for the dissolved oxygen concentration, c. $D^{\text{eff}}_{O_2,N}$ is the effective oxygen diffusion coefficient in Nafion within the agglomerate, and is obtained from the Bruggemann relation [38] as:

$$D^{\text{eff}}_{O_2,N} = \begin{cases} D_{O_2,N}\, \varepsilon^{1.5}_{\text{agg}} & \text{in nucleus} \\ D_{O_2,N} & \text{in coating} \end{cases} \tag{4}$$

The boundary condition for Eq. (2) must be posed at the interface with the gas pore. It requires equilibrium between the dissolved oxygen concentration in Nafion, c, and oxygen concentration in the gas pores, $c_{O_2,g}$, at the outer surface of the polymer coating [15], and is given by:

$$c_{\text{interface}} = \frac{c^*}{c^*_{O_2,g}} c_{O_2,g} = \frac{1}{H} c_{O_2,g} \tag{5}$$

where H is Henry's constant, and $c^*_{O_2,g}$ represents the concentration of oxygen at the cathode inlet. At the interior interface between the coating and the nucleus, continuity of oxygen concentration and oxygen flux must be satisfied.

One of the assumptions in the agglomerate scale model is that the overpotential remains constant within the agglomerate, *i.e.*, the ionic and electronic phase potentials do not vary within the agglomerate. This may be justified using a simple order-of-magnitude analysis. The potential drop from the center to the surface of a spherical agglomerate of diameter 1000 nm (the largest one considered here) using Ohm's Law is given by $\Delta\phi \approx i r_1/\sigma$, where i is the current density, r_1 is the radius of the agglomerate, and σ is either the electronic or protonic conductivity, depending on whether the protonic phase potential drop or the electronic phase potential drop is being considered. Using typical values of

$i = 10^4\,\mathrm{A\,m^{-2}}$, $r_1 = 500\,\mathrm{nm}$, and $\sigma = 10\,\mathrm{S\,m^{-1}}$ (for Nafion), we get $\Delta\phi = 0.05\,\mathrm{mV}$. This is the maximum possible potential drop in the ionic phase potential under any condition. For electron transport the potential drop is one order of magnitude lower. Since 0.05 mV is negligible (4 orders of magnitude lower) compared to the cell voltage of ~1 V, it can be safely neglected.

2.1.2. Numerical solution of agglomerate model equation

In order to solve Eq. (2) for an agglomerate of arbitrary shape, the finite-volume method is employed. In this method, the entire agglomerate is first discretized into small control-volumes. In this work, an unstructured mesh is used to allow flexibility of modeling any arbitrary agglomerate shape. The unstructured mesh is generated using the commercial mesh generation code CFD-GEOM™. In the finite-volume method, the governing equation [Eq. (2)] is first integrated over a representative control volume, O. This step is followed by application of the Gauss-divergence theorem, which, following procedures outlined elsewhere [39,40], yields a set of discrete algebraic equations of the following form

$$\sum_f \left[D^{\mathrm{eff}}_{\mathrm{O_2,N}f} \left(\frac{c_{\mathrm{N},f} - c_{\mathrm{O}}}{\vartheta_f} \right) A_f - \frac{J_{\mathrm{T},f} A_f}{\vartheta_f} \right] = -\gamma \frac{A_{\mathrm{v}} i_{\mathrm{s}}^{\mathrm{cat}} (1 - \varepsilon_{\mathrm{agg}})}{nF} V_{\mathrm{O}} = S_{\mathrm{O}} V_{\mathrm{O}} \tag{6}$$

where the summation is over all faces of the control volume, O. V_{O} is the volume of the control volume in question, and A_f is the surface area of each face of the control volume. $D^{\mathrm{eff}}_{\mathrm{O_2,N}f}$ is the diffusion coefficient of oxygen at the face, and is obtained from cell-center diffusion coefficients using distance-weighted interpolation. $c_{\mathrm{N},f}$ is the concentration at the cell center on the other side of face f, *i.e.*, the neighboring cell N, c_{O} is the concentration at cell O, and ϑ_f is the distance between the cell centers of the two cells straddling face f in the direction of the surface normal. $J_{\mathrm{T},f}$ represents the flux tangential on the face f, and the procedure to express it in terms of the cell-center concentrations may be found elsewhere [39,40].

Eq. (6) represents a set of coupled linear algebraic equations whose solution yields the cell-center concentrations at all cells within the entire agglomerate. This system of coupled algebraic equations was solved using the Generalized Minimum Residual Solver (GMRES) [41] with incomplete LU (ILU) pre-conditioning. Typically, 20 Krylov sub-spaces were used, and the residual was reduced by six orders of magnitude. Example of a sample unstructured mesh and the computed solution (dissolved oxygen concentration) is depicted in Fig. 4. This particular calculation was performed for an agglomerate of a pair of intersecting spheres with $r_1 = 1000\,\mathrm{nm}$, $r_2 = 600\,\mathrm{nm}$, an overlap parameter of $\xi = 0$, and with a coating of thickness $\delta = 60\,\mathrm{nm}$. It is clear from the figure that the mesh resolution used for such computations is quite high so as to accurately capture the oxygen concentration distribution, especially in the region where the spheres intersect. Grid independence studies revealed that any mesh with less than 500,000 cells is inadequate for such computations. In terms of computational effort, the mesh generation process was the primary consumer of CPU time. The mesh generation for each mesh required about 45 minutes of CPU time on a 3.2 GHz Intel Pentium4 processor, while the actual solution of the governing equation required less than 10 minutes in most cases.

2.1.3. Computation of volume-average quantities

Once the solution to the agglomerate-scale governing equation [Eq. (6)] has been obtained, it can be post-processed to extract quantities that appear as inputs to the device-scale CFD model, to be described in the next section.

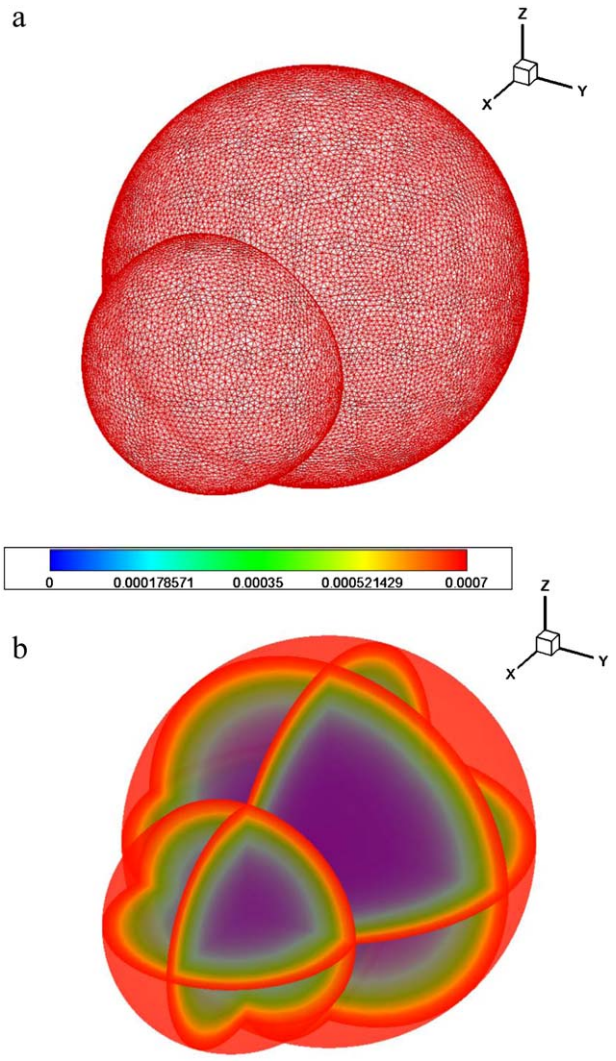

Fig. 4. Results from a demonstration case of the numerical solution of the generalized flooded agglomerate model equation: (a) a typical unstructured mesh comprised of 784,029 cells and (b) contours of O_2 concentration distribution (in $\mathrm{kmol\,m^{-3}}$).

In order to compute the effective properties for transport in the cathode catalyst layer, the volume fractions of the carbon–platinum solid clusters (ε_{S}), the proton-conducting polymer (ε_{N}), and the pores ($\varepsilon_{\mathrm{cat}}$), need to be calculated. Also, the total catalyst surface area per unit volume of cathode catalyst layer available for the oxygen reduction reaction (ORR), A_{v}, needs to be computed. These quantities are computed using the relationships presented in earlier publications [18,19,35], and are omitted here for the sake of brevity. Under the assumption that the agglomerate nucleus is made up of only the solid component and the polymer, the number of agglomerates per unit volume required to produce the solid component volume fraction, ε_{S}, is given by:

$$\widehat{n} = \frac{\varepsilon_{\mathrm{S}}}{V_{\mathrm{nuc}}(1 - \varepsilon_{\mathrm{agg}})} \tag{7}$$

where V_{nuc} is the volume of the agglomerate nucleus, and is computed directly by the agglomerate equation solver by summing up the volumes of all the control volumes that constitute the nucleus. Further, assuming that the entire polymer electrolyte (Nafion) in the cathode catalyst layer is only present either in the agglomerate nucleus or in the polymer coating around the agglomerate, the

volume fraction of the polymer electrolyte in the cathode can be obtained using

$$\varepsilon_N = \widehat{n}(V_{nuc}\varepsilon_{agg} + V_{ctg}) \tag{8}$$

where V_{ctg} is the volume of the polymer coating around the agglomerate nucleus, and is also computed directly by the agglomerate equation solver. Once the volume fractions of the solid component and the polymer are obtained, the porosity of the cathode catalyst layer is obtained using

$$\varepsilon_{cat} = 1 - \varepsilon_S - \varepsilon_N \tag{9}$$

The current per unit volume generated by the agglomerate, j_T^{agg}, is calculated using:

$$j_T^{agg} = \frac{\int_{V_{agg}} \gamma A_v i_s^{cat}(1-\varepsilon_{agg})dV}{V_{agg}} = -i_0^{ref}\left(\frac{c^*}{c_{O_2}^{ref}}\right)^{1-\alpha_T/n} \times \exp\left(-\frac{\alpha_T F}{RT}\eta\right)\frac{A_v(1-\varepsilon_{agg})}{c^*}\frac{\int_{V_{nuc}} c dV}{V_{agg}} \tag{10}$$

where V_{agg} is the total volume of the agglomerate (nucleus plus coating). The integral in the numerator of Eq. (10) is computed directly by the agglomerate equation solver by summing over the volume weighted concentration of each control volume. The current generated per unit volume of the cathode may be expressed in terms of the current generated per unit volume of the agglomerate as

$$j_T^{cat} = (1-\varepsilon_{cat})j_T^{agg} \tag{11}$$

As stated earlier, the quantity j_T^{cat} appears as a source in the governing equations for current conservation within the cathode, as will be discussed shortly.

2.2. Computational fluid dynamics (CFD) model

The sub-grid scale catalyst layer model, described in the preceding section, was implemented into a two-dimensional computational fluid dynamics (CFD) code that has been developed specifically for PEMFC applications, and has been validated [42] and successfully used in previous studies [35]. The purpose of this coupling is to enable prediction of the overall performance (polarization behavior) of the fuel cell by taking into account both local (agglomerate-scale) and global (device-scale) losses. The governing equations are the equations of conservation of mass (both overall and individual species), momentum, energy, and charge. For simplicity, it is assumed that the temperature does not change spatially, and thus, the energy conservation equation is not solved. Furthermore, it is assumed that water exists only in its vapor phase in gas diffusion layers and channels, and two-phase effects are not considered. The governing conservation equations are different inside and outside the membrane and are, therefore, presented here separately.

2.2.1. Channels, gas diffusion layers (GDL), and active catalyst layers (ACL)

The governing conservation equations for mass and momentum, at steady state, are written as [43–45]:

$$\text{overall mass}: \ \nabla\cdot(\varepsilon\rho\mathbf{U}) = \dot{S}_m \tag{12}$$

$$\text{momentum}: \ \nabla\cdot(\rho\varepsilon\mathbf{U}\mathbf{U}) = -\varepsilon\nabla p + \nabla\cdot(\mu_{eff}\nabla\mathbf{U}) + \frac{\mu\varepsilon^2\mathbf{U}}{\kappa} \tag{13}$$

$$\text{species mass}: \ \nabla\cdot(\rho\mathbf{U}Y_k) = -\nabla\cdot J_k + \dot{S}_k \quad \forall k = 1,2,\ldots,N \tag{14}$$

where ρ is the density, p is the pressure, μ is the dynamic viscosity of the fluid, and $\mathbf{U}$ is the fluid velocity vector. ε is the porosity of the medium and κ is the permeability. In Eq. (12), $\dot{S}_m$ is the mass source term due to electrochemical reactions, and is non-zero only in the catalyst layers. It results from the fact that a conservation equation for protons is not directly solved, and therefore, the mass of protons created or destroyed need to be added or subtracted out of the overall continuity equation. The last term in Eq. (13) represents the sub-grid scale drag force imposed by the pore walls on the fluid, written using the linear Darcy's Law [38]. In purely open regions, such as in the gas channels, $\varepsilon \to 1$ and $\kappa \to \infty$, and Eqs. (12) and (13) reduce to the well-known Navier–Stokes equations. In Eq. (14), Y_k is the mass fraction of the kth species, $\mathbf{J}_k$ is the mass diffusion flux of the kth species, and $\dot{S}_k$ is the production rate of the kth species due to electrochemical reactions. The total number of species in the system is denoted by N.

The diffusion flux of the kth species, $\mathbf{J}_k$, is modeled using the so-called dilute approximation [46]. By this approximation, the diffusion flux is written as

$$\mathbf{J}_k = -\rho D_{km}\nabla Y_k \tag{15}$$

where D_{km} is the free-stream diffusivity of species k into the mixture, and is henceforth denoted by D_k for simplicity. The free-stream diffusivity is given by the relation [46]:

$$D_{km} = D_k = \frac{1-X_k}{\sum_{\substack{i=1\\ i\neq k}}^{N}\frac{X_i}{\mathcal{D}_{ki}}} \tag{16}$$

where $\mathcal{D}_{ki}$ is the binary diffusivity of species k into species i, and X_k is the mole fraction of the kth species. Substitution of Eq. (15) into Eq. (14) yields the appropriate species transport equation under the dilute approximation formulation for open regions:

$$\nabla\cdot(\rho U Y_k) = \nabla\cdot(\rho D_k\nabla Y_k) + \dot{S}_k \quad \forall k = 1,2,\ldots,N \tag{17}$$

In porous regions, it is customary to use the so-called Bruggemann relation [38], and modify the free-stream diffusion coefficient, such that the governing species conservation equation becomes

$$\nabla\cdot(\varepsilon\rho U Y_k) = \nabla\cdot(\rho D_k\varepsilon^\tau\nabla Y_k) + \dot{S}_k \quad \forall k = 1,2,\ldots,N \tag{18}$$

where τ is the tortuosity of the porous region. Traditionally, a value of $\tau = 1.5$ is used in Eq. (18). In order to examine the effect of cathode structure and tortuosity on fuel cell performance, a more realistic tortuosity model, proposed by Abbasi et al. [47], is used. Hence the governing species conservation equation in the cathode catalyst layer becomes:

$$\nabla\cdot(\varepsilon_{cat}\rho U Y_k) = \nabla\cdot\left(\rho D_k\frac{\varepsilon_{cat}}{\tau_{cat}}\nabla Y_k\right) + \dot{S}_k \quad \forall k = 1,2,\ldots,N \tag{19}$$

where the tortousity, τ_{cat}, is given by [47]

$$\tau_{cat} = \frac{1}{\varepsilon_{cat}} + 1.196\frac{\sigma_{dev}}{\bar{d}} \tag{20}$$

where σ_{dev} is the standard deviation of the pore size in the cathode catalyst layer. In this study, a constant value of $\sigma_{dev} = 50$ nm has been used for the sake of convenience. $\bar{d}$ is the average pore size of the cathode catalyst layer, and is given by [48]:

$$\bar{d} = \frac{4}{3}\frac{\varepsilon_{cat}}{(1-\varepsilon_{cat})}r_{agg} \tag{21}$$

where r_{agg} is the radius of the equivalent sphere that has the same volume as the overlapping spheres used here.

The source due to the electrochemical reactions is non-zero only in the active catalyst layers of the anode and cathode, and is zero elsewhere. It is written as [49]

$$\dot{S}_k = \frac{j_T M_k}{2F} \tag{22}$$

where j_T is the net transfer current due to electrochemical reaction, M_k is the molecular weight of the kth species, and F is the Faraday constant. The anode transfer current j_T^{an} is expressed using the global single-scale Butler–Volmer equation [49]:

$$j_T^{an} = j_0 A_v^{an} \left[\exp\left(\frac{\alpha_a F}{RT}\eta\right) - \exp\left(-\frac{\alpha_c F}{RT}\eta\right) \right] \prod_{k=1}^{N} [\Lambda_k]^{\beta_k} \quad (23)$$

where j_0 is the reference current density, α_a and α_c are kinetic constants determined from experimentally measured Tafel plots. $[\Lambda_k]$ and β_k are the molar concentrations and the concentration exponents for the kth species, respectively. η is the electrode overpotential (including both activation and concentration overpotential) and is defined as the difference between the electronic or solid phase potential (ϕ_S) and the electrolyte or ionic phase potential (ϕ_F), *i.e.*, $\eta = \phi_S - \phi_F$. In this study, the above Butler–Volmer kinetic relation was used only for the anode and no multi-scale model was used, while the cathode transfer current was obtained from Eq. (11), following the multi-scale procedure outlined in Section 2.1.

In a PEMFC calculation, in addition to mass conservation, it is necessary to enforce charge conservation. Under the assumption of electro-neutrality, charge conservation reduces to current conservation, written as

$$\nabla \cdot \mathbf{i} = 0 \quad (24)$$

where $\mathbf{i}$ is the current density vector. In a PEMFC, the current flow is due to protons (H^+) flowing through the membrane, resulting in an ionic phase current ($\mathbf{i}_F$), and due to electrons flowing through the carbon in the porous matrix of the gas diffusion layers, resulting in an electronic phase current ($\mathbf{i}_S$). Thus, Eq. (24) can be rewritten as follows:

$$\nabla \cdot \mathbf{i}_F + \nabla \cdot \mathbf{i}_S = 0 \quad (25)$$

Since current transport in the ionic phase is due to ions and that in the electronic phase is due to electrons, the transport in each phase is governed by separate electric potential fields. Using Ohm's law, Eq. (25) can be written as

$$\nabla \cdot (\sigma_F \nabla \phi_F) + \nabla \cdot (\sigma_S \nabla \phi_S) = 0 \quad (26)$$

where σ_F and σ_S are the conductivities of the ionic and electronic phases, respectively. The exchange of current from the ionic to the electronic phase occurs due to electrochemical reactions during which electrons are transferred from one phase to the other. Thus, Eq. (26) can be rewritten as [44,49]:

$$-\nabla \cdot (\sigma_F \nabla \phi_F) = \nabla \cdot (\sigma_S \nabla \phi_S) = j_T \quad (27)$$

Eq. (27) represents two elliptic partial differential equations that are strongly coupled through the transfer current source. The ionic phase electric potential equation (for ϕ_F) must be solved in the active catalyst layer and the membrane, while the electronic phase electric potential equation (for ϕ_S) must be solved in the active catalyst layer (ACL) and the gas diffusion layer (see Fig. 1). In the active catalyst layer, both equations are solved, and are strongly coupled. The difference in value between ϕ_S and ϕ_F represents the total electrode overpotential.

2.2.2. Water and current transport in membrane

Nafion membranes are, for all practical purposes, impermeable to all gases except water. Thus, the governing equation for species transport outside the membrane [Eq. (14)] is irrelevant in this context. The only species that needs to be considered is water. For all other species, zero flux boundary conditions must be used at the membrane–ACL interface. Water transport in the membrane of a PEMFC occurs primarily due to diffusion and electro-osmotic drag, although there is some evidence that pressure-driven advection may also occur [50–54]. In phenomenological membrane models, it is customary to express water transport in terms of the water content, λ, as [55]:

$$\nabla \cdot \left[\eta_d \frac{\mathbf{i}}{F}\right] = \nabla \cdot \left[\frac{\rho_m}{M_m} D_\lambda \nabla \lambda\right] \quad (28)$$

The water content is defined as the ratio of the number of water molecules to the number of SO_3^- charge sites in the medium. In Eq. (28), it has been assumed that advective transport is negligible. D_λ denotes the diffusion coefficient of water in Nafion expressed in terms of the water content, η_d denotes the electro-osmotic drag coefficient, and ρ_m/M_m represents the molar density of the membrane. Fuller and Newman [56] give the diffusion coefficient as:

$$D_\lambda = (2.1 \times 10^{-7}) \times \lambda \times \exp\left[-\frac{2436}{T}\right] \quad (29)$$

where T is the absolute temperature. The electro-osmotic drag coefficient is given by [57]:

$$\eta_d = \frac{2.5}{22}\lambda \quad (30)$$

Current transport in the membrane is described by the ionic phase part of Eq. (27), except that there is no source, *i.e.*, the right hand side of the equation is zero. The ionic phase electrical conductivity of the membrane, σ_F, is again expressed by the empirical correlation [57]:

$$\sigma_F = 100 \exp\left[1268\left(\frac{1}{303} - \frac{1}{T}\right)\right] \sigma_{30} \quad (31)$$

where σ_{30} is the electrical conductivity of the membrane at 30 °C, and is given by [56]:

$$\sigma_{30} = 0.005139\lambda - 0.00326 \quad \text{for } \lambda > 1 \quad (32)$$

The ionic phase electrical conductivities in the anode catalyst layer and the cathode catalyst layer are evaluated using Eqs. (31) and (32) based on local values of water content. However, in these regions, the conductivities need to be corrected in order to account for the fact that the proton-conducting polymer is just one of the components in the layer. The effective ionic phase electrical conductivity in the cathode is given by Jaouen et al. [15], wherein non-overlapping spherical agglomerates are assumed. For the present study, the expression provided by Jaouen et al. [15] is modified to yield

$$\sigma_F^{cat} = (1 - \varepsilon_{cat}) \left[1 + \frac{\varepsilon_{agg} - 1}{\{(V_{agg}/V_{nuc})^{1/3} + a_1\}^3}\right] \sigma_F \quad (33)$$

where the constant a_1 has been introduced following Mazumder and Kamarajugadda [35] to ensure that in the case when the agglomerates do not have any coating, the effective protonic conductivity decays to zero. The constant a_1 is given by

$$a_1 = \min\left[0, \left\{\left(\frac{V_{agg}}{V_{nuc}}\right)^{1/3} + (1 - \varepsilon_{agg})^{1/3} - 2\right\}\right] \quad (34)$$

It is evident from Eqs. (28)–(32) that the two quantities that dictate the mass transport and electrical properties of a Nafion membrane are its water content and temperature. The water content is obtained by solution of the conservation equation for water [Eq. (28)]. However, solution of this equation requires specification of either the water content itself or the flux of water at the membrane–ACL interface, which in turn requires coupling with the rest of the computational domain. Various approaches for coupling the membrane with the overall calculation procedure and for implementation of the interface conditions are discussed in Kamarajugadda and Mazumder [42].

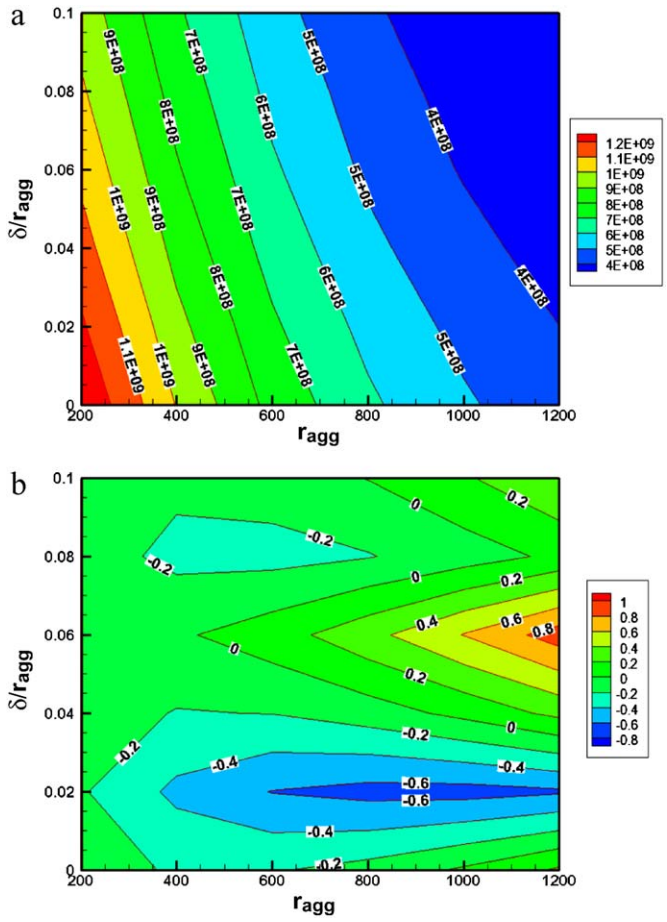

Fig. 5. Variation with agglomerate radius and polymer coating thickness of (a) numerically computed current generation per unit volume (in A m^{-3}) by spherical agglomerates and (b) percentage difference between numerical and analytical solution.

3. Results and discussion

Prior to performing full-scale CFD calculations to predict the performance of a PEMFC, validation of the numerical solution of the agglomerate scale equation was deemed necessary. Following this important step, the sub-grid scale model was implemented into the large-scale CFD model, and the effect of the agglomerate shape on the overall performance of the fuel cell was investigated. These studies are presented next.

3.1. Validation of the agglomerate scale model

The purpose of the sub-grid scale agglomerate model is to provide a measure of the volumetric current density generated by the agglomerates. Therefore, the numerical solution of the generalized flooded agglomerate model equation is validated against the analytical solution [15] for the current density generated by spherical agglomerates, before using it to analyze the effect of non-spherical agglomerate size and shape on overall fuel cell performance. Fig. 5(a) shows the volumetric current generation predicted by the numerical solution of the generalized flooded agglomerate model equation [Eq. (2)] for a large range of agglomerate radius and polymer coating thickness for nominal cathode overpotential value of $\eta = -0.5$ V, platinum loading of $m_{Pt} = 0.45$ mg cm^{-2}, Nafion volume fraction of $\varepsilon_{agg} = 0.4$, and platinum–carbon ratio of Pt|C = 0.28. Fig. 5(b) depicts the percentage difference between the numerical solution and the analytical solution [15]. It is clear from Fig. 5(b) that the numerical solutions are within ±1% of the analytical solutions for the entire range of agglomerate radius and coating thickness considered in this study. Although, the above results do not automatically prove the reliability of the numerical procedure for non-spherical shapes, based on the results of this single validation study, the generalized flooded agglomerate model can be used with some amount of confidence to predict current density generated by agglomerates of arbitrary shapes.

Table 1
Values of cathode model constants and properties.

Model parameter	Value/method of calculation
Transfer coefficient at cathode (Tafel constant)	1 (≥0.8 V) [18] 0.55 (<0.8 V) [18]
Reference exchange current density at cathode	1.288×10^{-4} A cm^{-2} (≥0.8 V) [18] 2.291×10^{-2} A cm^{-2} (<0.8 V) [18]
Diffusion coefficient of O_2 in Nafion	3.966×10^{-10} m^2 s^{-1} [18]
Henry's constant	10 [18]

3.2. Effect of agglomerate shape and size on local current generation

Following the validation studies, the generalized flooded agglomerate model was used to clearly elucidate the effect of agglomerate shape and size on the current density generated by agglomerates characterized as pairs of intersecting spheres. Agglomerate size was varied using three different values (200 nm, 600 nm, and 1000 nm) for the two radii (r_1, r_2) of the spheres. This gives rise to six different agglomerate configurations—three of which have equal sized overlapping spheres, and three of unequal sized overlapping spheres. For each of the above six cases, the agglomerate shape is further influenced by the distance between the two centers, which can be characterized by the overlap parameter (ξ). In this study, the overlap parameter was varied from −1 to +1. Also, in order to examine the effect of polymer coating, calculations for the current generated per unit volume for each of the above six configurations are conducted for agglomerates with no coating, with thin coating, and with capsule coating. The coating thickness for each agglomerate was calculated based on the radius of the larger of the two intersecting spheres using a value of $\delta/r_1 = 0.06$. All calculations discussed in this sub-section are carried out with a nominal cathode overpotential value of $\eta = -0.5$ V. The thickness of the cathode is assumed to be $L = 15$ μm, the polymer volume fraction within the agglomerate nucleus is $\varepsilon = 0.4$, the platinum mass loading is $m_{Pt} = 0.45$ mg cm^{-2}, and the platinum-to-carbon ratio in the catalyst ink is Pt|C = 0.28. Other relevant parameters used for these calculations are listed in Table 1. All calculations were performed assuming that the oxygen concentration in the gas pore surrounding the agglomerate to be equal to the oxygen concentration at the fuel cell cathode flow channel inlet. Evaluation of current generated per unit volume of agglomerate for other values of oxygen concentration is straightforward because of the linear dependence of the current density on the concentration distribution, as is evident from Eq. (10).

Since the number of parametric studies conducted [58] is too large to discuss extensively, only the important finding from this study is discussed here. The studies revealed that agglomerates of intersecting spheres resulted in a higher current generated per unit volume in comparison to spherical agglomerates of equivalent volume. The current generated per unit volume was found to correlate well with the surface-area-to-volume ratio of the agglomerate, and, for a given volume, intersecting spheres have a higher surface-area-to-volume ratio than spherical agglomerates. This is depicted in Fig. 6. In this figure, the normalization is with respect to a single sphere (the larger of the two radii, *i.e.*, r_1). It is clear from Fig. 6(b), that the current generation improves for an agglomerate comprised of intersecting spheres in comparison to a single sphere

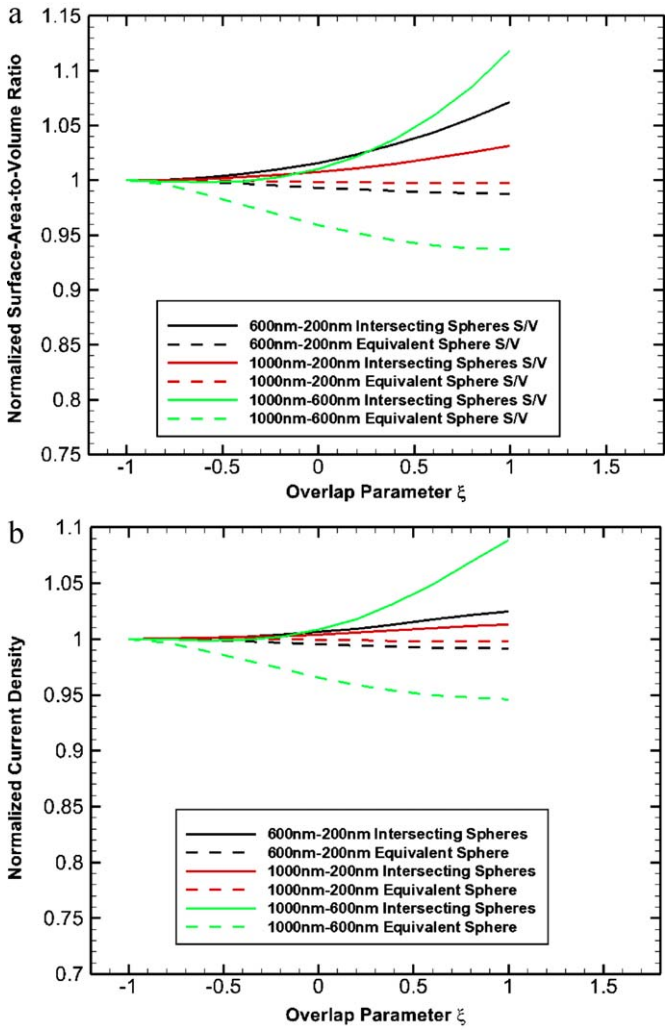

Fig. 6. Effect of agglomerate size and shape on (a) surface-area-to-volume ratio and (b) local current generated per unit volume.

of the same volume ("equivalent sphere"). The improvement is more pronounced for larger spheres than smaller ones because in smaller spheres, the mass transport resistances are not significant to begin with, and the entire agglomerate is almost saturated with the reactant (O_2). Further, comparison of Fig. 6(a) with Fig. 6(b) clearly illustrates that the current density correlates strongly with the surface-area-to-volume ratio of the agglomerate, although the relationship is not quite linear. While the results presented in Fig. 6 are for a case without coating, similar trends were obtained with both capsule and thin coating.

3.3. Effect of agglomerate shape and size on overall PEMFC performance

In addition to affecting the current density generated at the agglomerate scale, agglomerate shape and size affect global properties like cathode porosity, tortuosity, and proton conductivity, thereby affecting the overall fuel cell performance in more ways than one. For example, one of the findings of the studies described in the previous section is that the current generated by agglomerates without coating is larger than that generated by agglomerates with coating because of reduced mass transport resistance. However, lack of coating can cause difficulty in proton transport within the catalyst layer due to poor contact, as discussed in Section 2.2.2. Therefore, the results of the agglomerate scale modeling cannot be directly extrapolated to overall PEMFC performance. To gain a better understanding of the overall PEMFC performance, the results of the agglomerate scale model must be used in conjunction with larger length scale effects.

Table 2
Look-up table with current per unit volume generated by agglomerates of 200–200 nm intersecting spheres with $\xi = 0$ for various values of cathode overpotential.

Overpotential (V)	Volumetric current density ($A\,m^{-3}$)		
	No coating	Thin coating	Capsule coating
0	4.34852×10^{2}	3.72223×10^{2}	3.60637×10^{2}
−0.05	2.62150×10^{3}	2.24394×10^{3}	2.17409×10^{3}
−0.1	1.58036×10^{4}	1.35275×10^{4}	1.31065×10^{4}
−0.1404	6.74781×10^{4}	5.77596×10^{4}	5.59617×10^{4}
−0.1904	4.06774×10^{5}	3.48187×10^{5}	3.37349×10^{5}
−0.2404	2.45160×10^{6}	2.09847×10^{6}	2.03313×10^{5}
−0.2904	2.37045×10^{7}	2.02860×10^{7}	1.96534×10^{7}
−0.3404	6.31206×10^{7}	5.39983×10^{7}	5.23088×10^{7}
−0.3904	1.66735×10^{8}	1.42502×10^{8}	1.38006×10^{8}
−0.4404	4.31615×10^{8}	3.67993×10^{8}	3.56142×10^{8}
−0.4904	1.06647×10^{9}	9.04054×10^{8}	8.73617×10^{8}
−0.6	5.50848×10^{9}	4.49353×10^{9}	4.31027×10^{9}
−0.7	1.72047×10^{10}	1.27908×10^{10}	1.21477×10^{10}
−0.8	4.58003×10^{10}	2.80301×10^{10}	2.63290×10^{10}
−0.9	9.71473×10^{10}	4.52061×10^{10}	4.21920×10^{10}
−1	1.44451×10^{11}	5.51051×10^{10}	5.13459×10^{10}

Unlike the spherical flooded agglomerate model where a closed-form analytical expression for the volumetric current generated by an agglomerate is available, the generalized flooded agglomerate model requires calculation of the current density based on the numerical solution of the governing equation [Eq. (2)]. In other words, the generalized flooded agglomerate model provides data for current generated per unit volume of agglomerate for discrete combinations of the cathode overpotential (η), and the oxygen concentration ($c_{O_2,g}$) in the gas pore surrounding the agglomerates, even with the other cathode model parameters being held constant. Therefore, scaling and interpolation are necessary in order to obtain current density values for intermediate values of η and $c_{O_2,g}$ that are encountered during iterations in the numerical solution of the governing equations within the CFD model for PEMFCs. Accordingly, for each of the agglomerate configurations listed at the beginning of this sub-section, the generalized flooded agglomerate model was used to first create a look-up table of values of current generated per unit volume [using Eq. (10)] for various specified values of η ranging from zero to the open circuit potential, with an oxygen concentration equal to the concentration of oxygen at the fuel cell cathode flow channel inlet ($c^{*}_{O_2,g}$). Since the equation governing the oxygen reduction reaction within the agglomerate [Eq. (2)] is linear, the cathode current density at an arbitrary concentration of oxygen in the gas pore ($c_{O_2,g}$) can be simply obtained by scaling. Since the overpotential appears in the governing equation in an exponential form, logarithmic interpolation was found to produce better accuracy than linear interpolation. Sample look-up data that were generated using the sub-grid scale model is shown in Table 2.

The governing conservation equations of mass, momentum and current, described in Section 2.2, were solved using a conservative finite-volume technique [59]. The SIMPLE algorithm [59] was used to address pressure-velocity coupling in the Navier–Stokes equations. The 2D model, shown in Fig. 1, was used for simulations. All simulations were performed on a uniform grid with 50 cells in the axial direction and 150 cells in the cross-flow (y) direction. Nominally, 40 cells were used across each flow channel, 10 across each GDL, 5 across each active catalyst layer, and 40 across the membrane. This particular mesh size was chosen after a

Table 3
Simulation parameters and values of key properties at 323 K and 1/1 atm.

Model parameter	Value/method of calculation
Gas channel length	7.112 cm
Gas channel width	0.762 mm
Diffusion layer width	0.254 mm
Membrane width	0.175 mm
Membrane permeability	1.8×10^{-18} m^2
Diffuser and catalyst layer permeability	1.76×10^{-11} m^2
Membrane porosity	0.28
Anode and cathode diffuser layer porosity	0.5
Tortuosity for Bruggemann correlation	1.5
Air side/fuel side Pressures	1/1 atm.
Relative humidity of inlet streams	100%
Air side inlet N_2/O_2 molar ratio	79/21
H_2 stoichiometric flow	2.8 A cm^{-2} equivalent
O_2 stoichiometric flow	3.0 A cm^{-2} equivalent
Transfer coefficients at anode (Tafel constants)	0.5
Concentration dependence at anode	0.5 (H_2)
Reference current density at anode	1.6×10^{11} (A m^{-3}) (m^3/kmol H_2)$^{1/2}$
Membrane electrical conductivity	Springer et al. [57]
Diffuser layer electrical conductivity	100 (Ω^{-1} m^{-1})

rigorous grid-independence study, the details of which can be found in Kamarajugadda and Mazumder [42].

Moist hydrogen and moist air was introduced into the anode and cathode inlet, respectively. A plug velocity profile was imposed, and the magnitude of the velocity was calculated from a prescribed equivalent current density. For all simulations, the temperature was assumed to be 50 °C everywhere, and the energy equation was not solved. Other relevant parameters used for simulations are reported in Table 3. The kinetic constant, j_0, for the electrochemical reactions at the anode was determined by calibrating the current density at low bias voltage against experimental data reported by Ticianelli et al. [60,61]—a practice that has been used in the past [15,42]. All simulations were run with a prescribed bias voltage boundary condition rather than a prescribed current boundary condition.

All transport properties of the fluid, namely viscosity and binary diffusion coefficients, were computed using the Chapman–Enskog equations of kinetic theory [46,62]. The Lennard–Jones potentials, which are needed as inputs, were obtained from the CHEMKIN database. The density of the fluid was calculated using the ideal gas law. The solutions were deemed to be converged when the residuals of each of the equations decreased by seven orders of magnitude. In order to compute the actual cell voltage from the prescribed bias voltage (or potential loss), it is necessary to know the open circuit potential. As done by previous researchers [15,63], rather than use the Nernst potential, an empirical correlation [64] was used for the open circuit potential:

$$\phi_{OC} = 0.0025T + 0.2329 \quad (35)$$

This correlation results in an open circuit voltage of 1.04 V at 50 °C. Baseline values for cathode model parameters and properties are listed in Table 1.

Fig. 7 shows the predicted performance with cathodes comprised of agglomerates of intersecting spheres of equal radii. The overlap parameter chosen in all of these studies is $\xi = 0$, which represents the case where the center of the smaller sphere is on the surface of the larger sphere. All other cathode parameters are the same. For comparison, the predicted performance for agglomerates comprised of isolated spheres is also shown. The results indicate that when the agglomerate is small in size, the exact shape does not significantly affect the overall performance of the PEMFC. Furthermore, the shape of the ionomer (or polymer) coating around the nucleus is also found to be irrelevant, as also corroborated by the

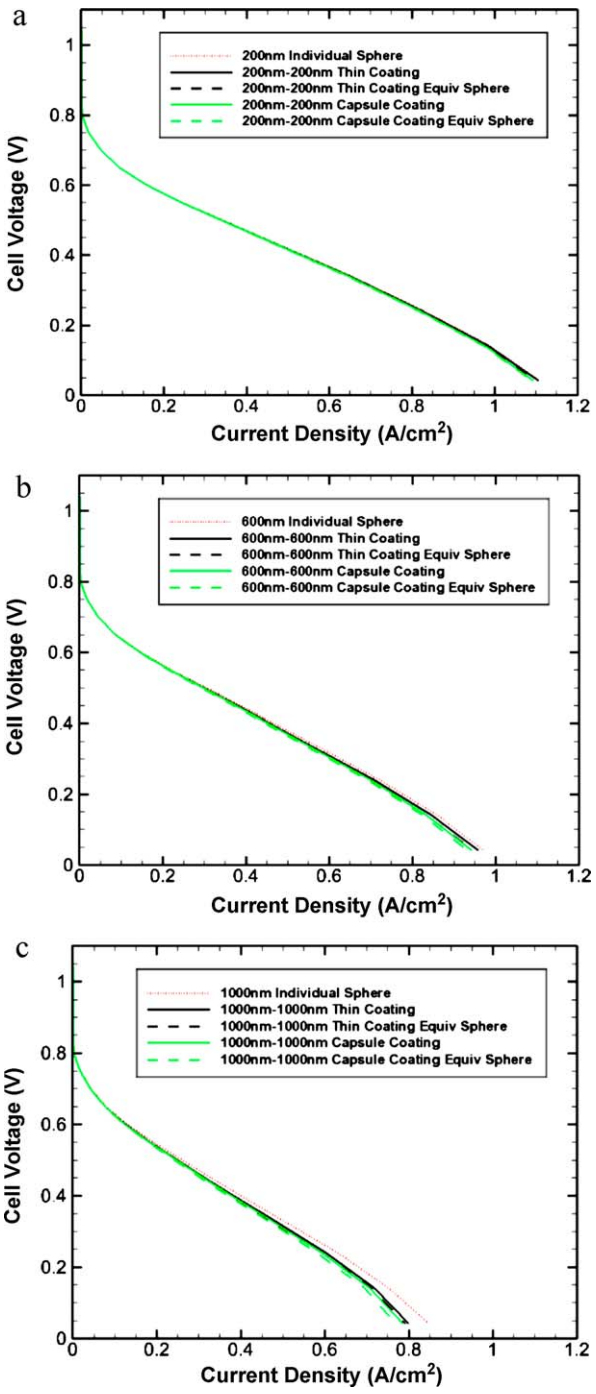

Fig. 7. Overall PEMFC performance predicted with cathodes comprised of agglomerates of various size and shape: (a) spheres of 200 nm radius, (b) spheres of 600 nm radius, and (c) spheres of 1000 nm radius.

data shown in Table 2. In this case, a coating thickness of $\delta/r_1 = 0.06$ was considered. When the agglomerate is large [as in Fig. 7(c)], both the shape of the nucleus and that of the coating plays a significant role in the performance at high current density (mass transport limited regime). In all cases, the intersecting spheres are found to result in better performance than a single equivalent sphere, in keeping with the results at the sub-grid scale (Section 3.2). Therefore, it may be concluded that the better performance for intersecting spheres is a direct result of increased current generation at the agglomerate scale due to increased surface-area-to-volume ratio of the agglomerate.

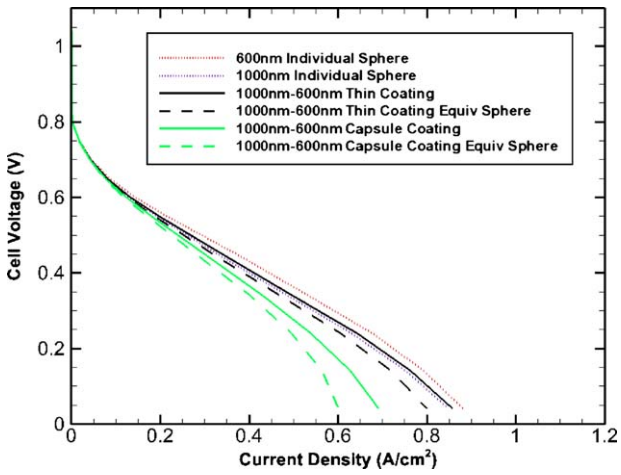

Fig. 8. Overall PEMFC performance predicted for agglomerates comprised of 1000–600 nm radii intersecting spheres with $\xi = 1$, and thin and capsule coatings.

Fig. 8 shows the predicted performance for cathodes comprised of agglomerates of intersecting sphere of unequal radii—in this case 1000 nm and 600 nm. An overlap parameter of $\xi = 1$ is chosen, which represents the nuclei of the two spheres just touching each other. At the agglomerate scale, this particular case demonstrated dramatic improvement in the current generated when compared to an equivalent sphere, as has been depicted in Fig. 6. Fig. 8 shows that the overall performance of the PEMFC is significantly affected by the shape of the agglomerate as well as the type of coating used. As in the sub-grid scale, the intersecting spheres result in better performance than an equivalent sphere of the same volume, primarily due to an increase in the surface-area-to-volume ratio. The thin coating produces significantly better performance than a capsule coating, particularly in the high current density regime. This stems from two issues. First, a thin coating poses less resistance than a capsule coating to the diffusion of dissolved oxygen to the reaction sites. Secondly, for the case of a capsule coating, the volume fraction of Nafion in the catalyst layer is significantly larger than in the case of a thin coating. Correspondingly, the volume fraction of the pores (average porosity, ε_{cat}) is significantly lower when a capsule coating is used. For example, for cathodes comprised of agglomerates of 1000–600 nm intersecting spheres, the porosity was calculated to be 0.19 with thin coating and only 0.07 with capsule coating. This poses additional mass transport resistance to the diffusion of oxygen within the pores of the cathode.

4. Summary and conclusions

With the advent of next-generation techniques for micro-/nano-fabrication, it will be possible to engineer fuel cell catalyst layers (electrodes) to desired compositions and structures. If a model is available that is general enough to answer the question, even qualitatively, as to what structure and composition is best for optimum performance, its impact on the advancement of fuel cell technology could be unprecedented. The model developed in this study is a logical extension of the popular isolated-sphere flooded agglomerate concept, and takes into account shape effects by considering intersecting spheres of unequal radii. Although intersecting spheres are investigated in this study based on what is observed in micrographs of catalyst layers, the model is applicable to agglomerates of any shape. The challenge is not so much of numerical solution, as of parameterizing the shape and relating it to an actual microstructure. Ultimately, the chosen parameters need to appropriately describe the real microstructure, or some statistical representation thereof. The new generalized sub-grid scale flooded agglomerate model requires numerical solution of the governing reaction-diffusion equation. This was accomplished using the unstructured finite-volume method. The model was first successfully validated against analytical solutions for a single spherical agglomerate. Following the validation phase, the effects of agglomerate shape and size on the overall performance (polarization behavior) of a polymer electrolyte membrane fuel cell were explored. Based on the results of these studies, the following two major conclusions may be drawn:

1. Cathodes comprised of agglomerates of intersecting spheres result in a better overall fuel cell performance than cathodes comprised of agglomerates of individual spheres of the same equivalent volume. This is a manifestation of the improvement in the oxygen reduction rate (or current generation rate) at the agglomerate scale due to increased surface-area-to-volume ratio.
2. For small agglomerate sizes, the spherical flooded agglomerate model with isolated equivalent spheres (as used in all previous studies using the flooded agglomerate model) appears to be an acceptable approximation even when the agglomerates are not strictly spherical in shape. In other words, shape effects are insignificant when the agglomerates are small. However, for larger agglomerates (>600 nm radius), shape effects are significant, and a model that accounts for the shape of the agglomerate, as the one proposed here, is necessary for accurate prediction of PEMFC performance.

In the future, the study will be extended to include the effect of liquid water and non-isothermal effects. However, the authors hope that this study has been able to provide some directions for future improvements in modeling the cathode of a PEMFC without actual microstructure reconstruction.

Acknowledgment

ESI Inc. is gratefully acknowledged for providing free licenses for their commercial mesh generation package CFD-GEOM™.

References

[1] R. O'Hayre, D. Barnett, F. Prinz, Journal of the Electrochemical Society 152 (2) (2005) A439–A444.
[2] M. Zhu, X.-Z. Xu, R. Su, J.-M. Yang, Journal of the Electrochemical Society 152 (3) (2005) A511–A515.
[3] G. Sasikumar, J. Ihm, H. Ryu, Journal of Power Sources 132 (2004) 11–17.
[4] Z. Xie, T. Navessin, K. Shi, R. Chow, Q. Wang, D. Song, B. Andreaus, M. Eikerling, Z. Liu, S. Holdcroft, Journal of the Electrochemical Society 152 (6) (2005) A1171–A1179.
[5] D. Song, Q. Wang, Z. Liu, T. Navessin, M. Eikerling, S. Holdcroft, Journal of Power Sources 126 (2004) 104–111.
[6] C. Marr, X. Li, Journal of Power Sources 77 (1999) 17–27.
[7] A. Kulikovsky, J. Divisek, A. Kornyshev, Journal of the Electrochemical Society 146 (11) (1999) 3981–3991.
[8] M. Secanell, B. Carnes, A. Suleman, N. Djilali, Electrochimica Acta 52 (7) (2007) 2668–2682.
[9] D.H. Schwarz, N. Djilali, Journal of the Electrochemical Society 154 (11) (2007) B1167–B1178.
[10] T. Springer, I. Raistrick, Journal of the Electrochemical Society 136 (6) (1989) p1594.
[11] S.J. Ridge, R.E. White, Y. Tsou, R.N. Beaver, G.A. Eisman, Journal of the Electrochemical Society 136 (7) (1989) 1902–1909.
[12] M.L. Perry, J. Newman, E.J. Cairns, Journal of the Electrochemical Society 145 (1) (1998) 5–15.
[13] P.-C. Sui, L.-D. Chen, J. Seaba, Y. Wariishi, Modeling and optimization of a PEMFC catalyst layer, SAE Technical Paper, Number 1999-01-0539, 1999.
[14] M. Eikerling, A. Kornyshev, Journal of Electroanalytical Chemistry 475 (1999) 107–123.
[15] F. Jaouen, G. Lindbergh, G. Sundholm, Journal of the Electrochemical Society 149 (4) (2002) A437–A447.
[16] F. Jaouen, G. Lindbergh, K. Wiezell, Journal of the Electrochemical Society 150 (12) (2003) A1711–A1717.

[17] L. Pisani, M. Valentini, G. Murgia, Journal of the Electrochemical Society 150 (12) (2003) A1549–A1559.
[18] W. Sun, B.A. Peppley, K. Karan, Electrochimica Acta 50 (2005) 3359–3374.
[19] M. Secanell, K. Karan, A. Suleman, N. Djilali, Electrochimica Acta 52 (22) (2007) 6318–6337.
[20] N. Siegel, M. Ellis, D. Nelson, M. Von Spakovsky, Journal of Power Sources 128 (2004) 173–184.
[21] H. Gasteiger, J. Panels, S. Yan, Journal of Power Sources 127 (2004) 162–171.
[22] K. Jeng, C. Kuo, S. Lee, Journal of Power Sources 128 (2004) 145–151.
[23] Z. Farhat, Journal of Power Sources 138 (2005) 68–78.
[24] K.-M. Yin, Journal of the Electrochemical Society 152 (3) (2005) A583–A593.
[25] C.-Y. Jung, C.-H. Park, Y.-M. Lee, W.-J. Kim, S.-C. Yi, International Journal of Hydrogen Energy 35 (16) (2010) 8433–8445.
[26] M. Srinivasrao, D. Bhattacharyya, R. Rengaswamy, S. Narasimhan, International Journal of Hydrogen Energy 35 (12) (2010) 6356–6365.
[27] S. Obut, E. Alper, Journal of Power Sources 196 (4) (2011) 1920–1931.
[28] Y. Tabe, M. Nishino, H. Takamatsu, T. Chikahisa, Journal of the Electrochemical Society 158 (10) (2011) B1246–B1254.
[29] G. Wang, P.P. Mukherjee, C.-Y. Wang, Electrochimica Acta 51 (2006) 3139–3150.
[30] P.P. Mukherjee, C.-Y. Wang, Journal of the Electrochemical Society 153 (5) (2006) A840–A849.
[31] K. Lange, P.C. Sui, N. Djilali, Journal of the Electrochemical Society 157 (10) (2010) B1434–B1442.
[32] K. Lange, P.C. Sui, N. Djilali, Journal of Power Sources 196 (6) (2011) 3195–3203.
[33] N.A. Siddique, F. Liu, Electrochimica Acta 55 (19) (2010) 5357–5366.
[34] F. Jaouen, Electrochemical characterization of porous cathodes in the polymer electrolyte fuel cell, Ph.D. Thesis, Kungl Tekniska Hogskolan, Stockholm, 2003.
[35] S. Kamarajugadda, S. Mazumder, Journal of Power Sources 183 (2) (2008) 629–642.
[36] J. Larminie, A. Dicks, Fuel Cell Systems Explained, second ed., Wiley, 2003.
[37] P. Jain, L.T. Biegler, M.S. Jhon, Journal of the Electrochemical Society 157 (8) (2010) B1222–B1229.
[38] M. Kaviany, Principles of Heat Transfer in Porous Media, Springer-Verlag, 1991.
[39] A.W. Date, Introduction to Computational Fluid Dynamics, Cambridge University Press, 2005.
[40] A. Kumar, S. Mazumder, International Journal for Numerical Methods in Fluids 64 (4) (2010) 409–442.
[41] Y. Saad, Iterative Methods for Sparse Linear Systems, second ed., SIAM, Philadelphia, PA, 2003.
[42] S. Kamarajugadda, S. Mazumder, Computers and Chemical Engineering 32 (7) (2008) 1650–1660.
[43] S. Dutta, S. Shimpalee, J.W. Van Zee, International Journal of Heat and Mass Transfer 44 (11) (2001) 2029–2042.
[44] S. Mazumder, J.V. Cole, Journal of the Electrochemical Society 150 (11) (2003) A1503–A1509.
[45] S. Mazumder, J.V. Cole, Journal of the Electrochemical Society 150 (11) (2003) A1510–A1517.
[46] R.B. Bird, W. Stewart, E.N. Lightfoot, Transport Phenomena, second ed., Wiley, New York, 2001.
[47] M.H. Abbasi, J.W. Evans, I.S. Abramson, AIChE Journal 29 (4) (1983) 617–624.
[48] D.G. Huizenga, D.M. Smith, AIChE Journal 32 (1) (1986) 1–6.
[49] J.S. Newman, Electrochemical Systems, Prentice-Hall, New York, 1973.
[50] G. Janssen, Journal of the Electrochemical Society 148 (12) (2001) A1313–A1323.
[51] A. Weber, J. Newman, Journal of the Electrochemical Society 150 (7) (2003) A1008–A1015.
[52] A. Weber, J. Newman, Journal of the Electrochemical Society 151 (2) (2004) A311–A325.
[53] A. Weber, J. Newman, Journal of the Electrochemical Society 151 (2) (2004) A326–A339.
[54] T. Thampan, S. Malhotra, H. Tang, R. Datta, Journal of the Electrochemical Society 147 (9) (2000) 3242–3250.
[55] S. Mazumder, Journal of the Electrochemical Society 152 (8) (2005) A1633–A1644.
[56] T. Fuller, J. Newman, Journal of the Electrochemical Society 140 (5) (1993) 1211–1225.
[57] T.E. Springer, T.A. Zawodzinski, S. Gottesfeld, Journal of the Electrochemical Society 138 (8) (1991) 2334–2342.
[58] S. Kamarajugadda, Advanced models for predicting performance of polymer electrolyte membrane fuel cells, Ph.D. Dissertation, Mechanical Engineering, The Ohio State University, 2011.
[59] S.V. Patankar, Numerical Heat Transfer and Fluid Flow, Hemisphere Publishing Corporation, Washington D.C, 1980.
[60] E.A. Ticianelli, C.R. Derouin, S. Srinivasan, Journal of Electroanalytical Chemistry 251 (2) (1988) 275–295.
[61] E.A. Ticianelli, C.R. Derouin, A. Redondo, S. Srinivasan, Journal of the Electrochemical Society 135 (9) (1988) 2209–2214.
[62] J.O. Hirschfelder, C.F. Curtiss, R.B. Bird, Molecular Theory of Gases and Liquids, Wiley, New York, 1954.
[63] V. Gurau, H. Liu, S. Kakac, AIChE Journal 44 (11) (1998) 2410–2422.
[64] A. Parthasarathy, S. Srinivasan, A.J. Appleby, Journal of the Electrochemical Society 139 (9) (1992) 2530–2537.